International Journal for Housing Science and Its Applications
Publish August 4, 2025. Volume 46, Issue 3 Pages 1600-1607

https://doi.org/10.70517/ijhsa463123

# Structure optimization algorithm-based study on the regulation of mechanical properties and biological response of cross-linked hydrogels in drug delivery systems

**Wenda Zhang**[1,*]
[1] School of Aerospace, Transport and Manufacturing, Cranfield University, Cranfield, MK43 0AL, UK
Corresponding authors: (e-mail: wendazh0523@outlook.com).

**Abstract** Enhancing drug delivery requires improving the quality of cross-linked hydrogels. In this paper, a molecular generation model is constructed based on graph convolutional neural network (GCNN). By simulating the intermolecular interaction situation and network structure, we optimize the selection of cross-linking agent and chain segment design to enhance the mechanical properties of hydrogels under different ratios. Systematically carry out hydrogel preparation and characterization tests to analyze the crystalline structure and thermal stability of borax-pectin cross-linked (SICH) hydrogels. The behavior and effect of SICH hydrogels based on structure optimization algorithms in drug delivery are analyzed through drug delivery practice. The results showed that the cell viability of SICH hydrogels in drug delivery was at least 70.49% with low cytotoxicity.The in vivo drug release of SICH hydrogels was nearly three times higher than that of PVA hydrogels in 24 hours. For in vitro drug release, it released up to 86.68% in 24 hours in a smooth manner, which had a good drug modulation release effect. Stable and efficient drug delivery can be achieved using cross-linked hydrogel SICH.

**Index Terms** GCNN, molecular generation model, SICH hydrogel, crystalline structure, thermal stability, drug delivery

## I. Introduction

Hydrogels are a class of polymers with an extremely hydrophilic three-dimensional network structure, usually crosslinked by hydrophilic macromolecules, which are able to absorb liquids tens to thousands of times its own mass to dissolve without dissolving [1]. In the field of drug release, the high porosity enables the loading of drugs into hydrogel scaffolds, and by controlling the degree of cross-linking of the hydrogel the pore size and connectivity can be adjusted to control the rate of drug release [2], [3]. A better understanding of the mechanical properties and drug response of hydrogel structures is a necessary step for their clinical application.

Based on the crosslinked network forces, hydrogels can be categorized into physical hydrogels, chemical hydrogels and composite hydrogels. Physical cross-linked hydrogels are formed through physical interactions [4]. The cross-linking process of this type of hydrogel relies on weak physical forces and has the advantages of low cost, low cytotoxicity, and simple operation, but the reversibility of its cross-linking process often leads to the problem of insufficient mechanical strength of the hydrogel [5]-[7]. Chemically crosslinked hydrogels are hydrogels that form permanent, irreversible covalently bonded crosslinked structures through chemical reactions [8]. The three-dimensional network structure of chemically crosslinked hydrogels is made up of polymer chains tightly linked to each other by covalent bonds, giving the hydrogel high mechanical strength and stability [9], [10]. The forces constituting the composite hydrogel, on the other hand, contain both physical and chemical actions [11]. This weak and brittle drawback of conventional hydrogels has greatly limited the application of hydrogels in many applications [12]. Therefore, by exploring the structure-optimized preparation method of crosslinked hydrogels, the deformation mode of hydrogel limbs as well as the multidimensional regulation of deformation kinetics are of great significance for their drug delivery function in biomedical scenarios [13]-[16].

The mechanical properties and biological response characteristics of cross-linked hydrogels will directly affect their effectiveness in drug delivery systems. In this paper, in order to realize the effective regulation of crosslinked hydrogels in drug delivery, a molecular generation model based on structure optimization algorithm is proposed to improve the drug delivery effect of crosslinked hydrogels. The molecular generation model based on the structure optimization algorithm simulates, predicts and optimizes the interactions between hydrogel molecules to find the optimal molecular structure. Crosslinked hydrogels are prepared by experimental preparation techniques and their characterization is carried out to excavate the molecular optimization of crosslinked hydrogels. The crosslinked

hydrogels were applied to rat ex vivo and ex vivo drug delivery experiments to analyze their ex vivo and ex vivo drug release.

## II. Research on the design and performance regulation of cross-linked hydrogel based on structure optimization algorithm

This chapter constructs a molecular generation model based on molecular structure optimization algorithm. It also analyzes the crystalline structure characterization and thermodynamic property characterization of cross-linked hydrogels after preparing cross-linked hydrogels as experimental materials.

### *II. A.Molecular graph-based molecular generation models*

In recent years, molecular generative modeling based on graph neural networks has demonstrated powerful design capabilities in the fields of chemistry and materials. By simulating intermolecular interactions and network topologies, such algorithms can provide theoretical support for the molecular design of cross-linked hydrogels, guiding steps such as cross-linker selection and chain segment optimization to efficiently regulate mechanical properties and biological responses.

Generative models based on text sequences have been well established in many generative and design tasks with good application and performance capabilities. However, mainstream algorithms are still using SMILES, a not-so-robust molecular representation, and its inherent limitations affect the performance of downstream molecular generative models. This has prompted recent research to turn to molecular graph methods that are more expressive for molecules. Graph generative models have specific advantages in the field of molecular generation. The construction of this class of generative models focuses on solving the following 2 problems:

1) Designing neural network architectures that can directly process graph data structures;

2) Designing the process of generating molecular graphs.

In this class of work, molecules are generally represented as undirected graphs. In this, atoms and chemical bonds in a molecule are represented as nodes and edges in the graph, respectively. The characterization of the molecular structure is done by the adjacency tensor as well as by the node identity matrix X (which is used to represent the type of atom, e.g., oxygen, fluorine, etc.). The molecule generation problem can thus be translated into generating graphs that represent valid molecules, and there are typically 2 processes for generating molecular graphs for such models:

(1) Sequential generation of molecular graphs - constructed by adding nodes (atoms) and edges (bonds) one by one;

(2) One-step generation of the complete molecular graph.

Graph Neural Networks (GNN) served as the infrastructure for processing such data structures. Numerous GNN variants have since emerged, and most of these architectures have been applied to molecular generation tasks in the last few years. The general GNN architecture is obtained by stacking several propagation blocks based on a nonlinear propagation rule. The formula is given below:

$$H^{l+1} = f_{PROP}(H^l, E) \forall l \in L \tag{1}$$

where $H^l$ and $H^{l+1}$ are the hidden variables (characterization of the graph level) at the $t$ th and $t+1$ th layers, respectively, $f_{PROP}$ is the graph characterization operator (the forward propagation function), and $E$ is the connectivity information (i.e., direction of information delivery) of the graph.

Generative models applied to molecular graphs have undergone continuous development and experimentation, resulting in graph generative model architectures that cope with a variety of molecular generation problems. An early and more representative network architecture for processing graphs is the graph convolutional neural network (GCNN), a class of network architectures commonly used in the processing of graph data structures.The effect of GCNN is similar to that of the convolutional neural networks applied to Euclidean structured data (e.g., images), which were first applied to the processing of molecular information.The performance of the GCNN in many molecular prediction tasks is better than that of the traditional Morgan molecular fingerprinting (e.g., ECFP). In principle, GCNN can be regarded as a class of trainable molecular fingerprints. The GCNN is then applied to tasks related to quantum chemical computing. In order to integrate 3D molecular information in molecular maps, a deep tensor neural network was developed. This network architecture treats the 3D molecular structure as a fully connected graph with weights and performs graph convolution operations on this data structure, after which the model is applied to a variety of quantitative computational tasks. The GCNN combined with a matching network (MN) is applied to a small number of samples, and the results show that this architecture performs better than traditional molecular fingerprinting-based methods for small-sample classification tasks. A large-scale comparative analysis of different types of machine learning algorithms on different benchmark datasets reveals that GCNN significantly outperforms other

types of algorithms (e.g., Graph Attention Networks) on many tasks. All of the above work demonstrates the superior performance of GCNN on the task of extracting relevant representations of molecular structures. Thus for graph generation models, GCNN is a preferred class of solutions. Taking crosslinked hydrogels as an example, in this study, the crosslinking process of borax and pectin is simulated by GCNN model, which can predict the stress-strain behavior of hydrogels with different X-values (borax content) and thus optimize the synthesis parameters.

### *II. B.Preparation of cross-linked hydrogels*

#### II. B. 1) Synthesis of SICH hydrogels

First, different concentrations of borax powder were dissolved in 150 mL of deionized water to obtain the borax solution. Then 2.5 g of pectin powder was weighed and poured into the dissolved borax solution, and stirred with a magnetic stirrer until the pectin powder was fully dissolved to obtain a mixed solution of pectin and borax. Afterwards, the mixed solution was poured into a glass dish and spread out, and dried in an oven to 35% of the original mass of the hydrogel to obtain a pectin hydrogel film. Finally, the resulting pectin hydrogel film was diffused into 0.15 M zinc acetate solution for 10 min to obtain SICH hydrogel with excellent mechanical strength and good electrical conductivity. In this paper, the synthesized pectin hydrogels were noted as SICH-X according to the different ratios of borax. X is the content of borax. In addition, SICH-Cu was synthesized using copper sulfate solution instead of zinc acetate solution during the synthesis. SICH-G/W hydrogels were prepared by soaking the SICH hydrogels in glycerol/water solution for 15 h. The ratio of glycerol to water was l:1. Pure pectin hydrogel was prepared by weighing 2.5 g of pectin powder dissolved in 150 mL of deionized water and then dried to 35% of the solution mass. Pectin-Zn was prepared by immersing pure pectin hydrogel in zinc acetate solution after 30 min crosslinking.

#### II. B. 2) Preparation of polyvinyl alcohol (PVA) hydrogels

First, 15 g of PVA powder was added to 150 mL of deionized water and stirred in a water bath at 100 °C until the PVA powder was fully dissolved to form a PVA solution. Second, the prepared PVA solution was poured into a glass dish and spread out. Then it was frozen by freeze-thaw cycle method at -25°C, crosslinked for 15 h, and finally thawed at 30°C. The PVA hydrogel was obtained by three freeze-thaw cycles.

#### II. B. 3) Physicochemical properties testing of SICH hydrogels

The surface morphology of the hydrogels was observed using a ZeissSigma300 scanning electron microscope (SEM) at an accelerating voltage of 12 kV. Prior to the observation, the hydrogel samples were freeze-dried, sliced using a freeze-dryer, and fixed on a fixture with a conductive adhesive. To ensure conductivity, the samples were coated with gold. A magnification of 120x was used for the measurements.

The results of pectin, pectin-Zn and SICH hydrogels were validated using Fourier transform infrared spectroscopy (FTIR). The hydrogel samples were lyophilized and milled in liquid nitrogen, and the dried sample powder was homogeneously mixed with potassium bromide particles and scanned against a blank potassium bromide particle background. All spectra were obtained at room temperature after 35 scans with a resolution of 4 $cm^{-1}$ and a range of 450 to 4500 $cm^{-1}$.

Pectin, pectin-Zn and SICH, and PVA hydrogels were analyzed by X-ray photoelectron spectroscopy (XPS) using an ESCALabMKII X-ray photoelectron spectrometer. The temperature tests were carried out in the range of 0 °C to 60 °C.

Thermogravimetric analysis (TGA) of SICH hydrogels was performed by scanning the temperature range from 0°C to 800°C under airflow conditions.

Differential scanning calorimetry (DSC) heating and cooling curves were collected by scanning under nitrogen flow from 0°C to 300°C using TADSC250.

#### II. B. 4) Testing of mechanical properties of SICH hydrogels

In this study, tensile and cyclic tests were performed on a tensile testing machine (AGS-X). In the tensile and cyclic tests, all samples were in dumbbell shape with a tensile rate of 25 mm/min. the modulus of elasticity was calculated from the slope of the initial linear region (s=15-25%) of the stress-strain curve of the hydrogel. The toughness value was the integral of the stress-strain curve. The test was repeated three times for all samples.

#### II. B. 5) Conductivity testing of SICH hydrogels

The electrochemical impedance spectra of pectin hydrogels were measured using an electrochemical workstation (CHI660E) at 10-6-10-1 Hz with a voltage of 150 mV. The pectin hydrogel was sandwiched between two stainless steel sheets and the ionic conductivity of the pectin hydrogel was calculated by the following equation.

$$\sigma = \frac{L}{RA} \tag{2}$$

where L is the thickness of the pectin hydrogel (in m), R is the resistance (in $\Omega$), and A is the contact area of the pectin hydrogel (in m²).

### *II. C. Cross-linked hydrogel structure and property characterization*

#### II. C. 1) Crystalline structure characterization

From the Fourier Transform Infrared (FTIR) results, it was known that there were crystalline regions in the prepared crosslinked hydrogels, so X-ray diffraction (XRD) was used to further investigate the crystalline structure. Figure 1 shows the XRD results. From Fig. 1(a), it can be seen that PVA shows an amorphous structure, while SICH has the strongest diffraction peak at 17.08°, which corresponds to the characteristic crystallization peaks of the crystalline surface of SICH.S1-S4 (the gluing hydrogels, representing the initial linear regions of the stress-strain curves of the different proportions of the hydrogels) retained the characteristic peaks of the crystallization of SICH such as the peaks at 17.08° and the characteristic peaks at the vicinity of 39.11°, but are different from those of pure SICH. However, compared with pure SICH, the diffraction intensity of S1-S4 is significantly lower at both characteristic peaks, especially the crystallization peak at 17.08°; In addition, the characteristic peak of S1-S4 near 39.11° is displaced to a large angle, which confirms that the crystalline structure in S1-S4 changes during freeze-thaw cycling due to interactions such as hydrogen bonding between the PVA chain segments and the SICH chain segments.

The crystallinity (Xc) of the crosslinked hydrogels can be calculated based on the ratio of the area of the crystalline zone to the area and sum of the amorphous zone of the crystalline zone. Compared with pure SICH, the crystallite size of S1-S4 was significantly reduced, from which it can be inferred that in the process of forming S1-S4, the interaction between the PVA chains and the SICH chains may disturb the arrangement order of the SICH chains, and the structure of the SICH folded chains at the point of action was disrupted, and the crystalline area of the SICH became smaller, and more polymer chains were bound in the crystalline area of the SICH.

The XRD spectra of pectin-Zn and L1-L4 (representing different pectin hydrogel thicknesses) are shown from Fig. 1(b). As can be seen from the figure, pectin-Zn also shows an amorphous structure. Comparing the XRD spectra of S1-S4 and L1-L4, it can be found that the XRD spectra of L1-L4 are similar to those of S1-S4, and L1-L4 also still maintains the basic crystalline characteristic peaks of SICH, which implies that there are still some SICHs in L1-L4 that form the crystalline regions through folded chains arranged parallel to each other. However, compared with S1-S4, the diffraction peaks of L1-L4 are broader and flatter in intensity near 18.4° and 39.66°. The Xc of L1-L4 was calculated based on the ratio of the area of the crystalline region to the area of the amorphous region and of the crystalline region.Combined with the data of crystallinity and grain size, it can be seen that the crystallinity and crystalline size of L1-L4 are smaller than those of S1-S4, which suggests that the loading of pectin-Zn reduces the crystallinity of SICH, which may be due to the fact that in the process of forming L1-L4, the interaction between the pectin-Zn and the SICH interaction interfered with the crystalline structure of SICH chains.

The XRD results confirmed that PVA and SICH formed cross-linked hydrogels with a three-dimensional network structure through hydrogen bonding interactions, and pectin-Zn was successfully loaded in L1-L4 and interacted with PVA and/or SICH, such as hydrogen bonding and electrostatic interactions.

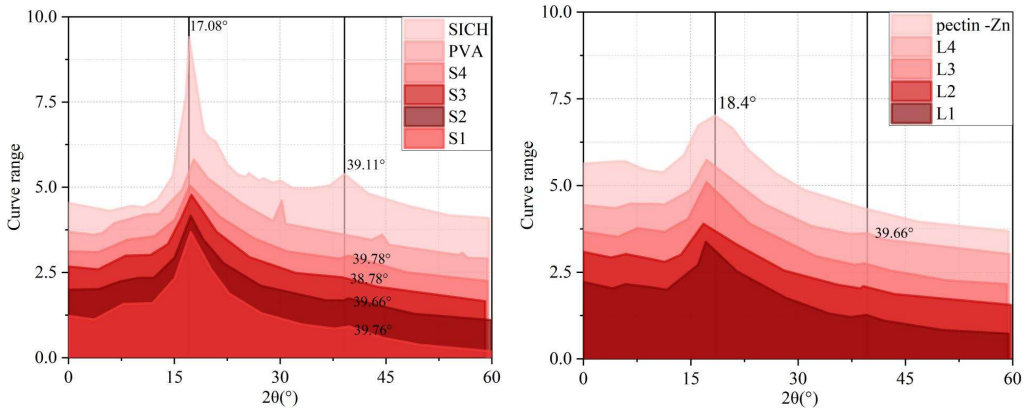


(a) XRD patterns of SICH, PVA and composite hydrogel

(b) XRD patterns of pectin -Zn and composite hydrogel

Figure 1: XRD pattern

**II. C. 2) Characterization of thermodynamic properties**

Figure 2 shows the thermogravimetric analysis (TGA) curves of SICH, PVA, pectin-Zn, and crosslinked hydrogels, from which it can be observed that the trend of the TG curves of the crosslinked hydrogels is in agreement with that of SICH. Due to the dehydration of the crosslinked hydrogel, the thermal weight loss of the first stage of SICH and crosslinked hydrogel occurred before 300 °C. It is noteworthy that the weights of SICH and crosslinked hydrogel do not change with increasing temperature in the temperature range of 83-222 °C, suggesting that there is a phase change of SICH in this temperature range, which is related to the melting process of SICH crystallization.

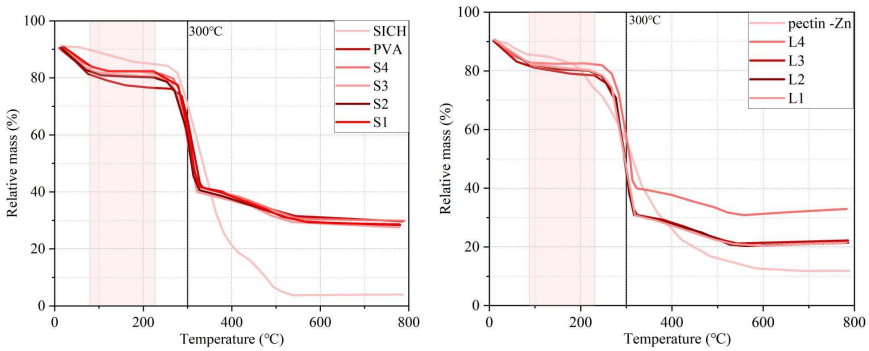


(a) TGA curves of SICH, PVA and cross-linked hydrogels

(b) TGA curves of pectin -Zn and cross-linked hydrogels

Figure 2: TGA curves of SICH, PVA, pectin -Zn and cross-linked hydrogels

Differential scanning calorimetry (DSC) tests were performed to further investigate the thermal properties of the cross-linked hydrogels. Figure 3 shows the DSC profiles of SICH, PVA, pectin-Zn and cross-linked hydrogels. As can be seen from the DSC profiles in Fig. 3, the unchanged phase of heat loss shown by the TG curve corresponds to the position of the melting peak of SICH in the DSC curve. Compared with SICH, the intensities of both S1-S4 (between temperatures of 75 °C and 125 °C, corresponding to the part of the elliptical region in the figure) and L1-L4 (between temperatures of 175 °C and 225 °C, corresponding to the part of the elliptical region in the figure) at this melting heat absorption peak were significantly decreased, which was related to the change of crystallization of SICH in the crosslinked hydrogel.

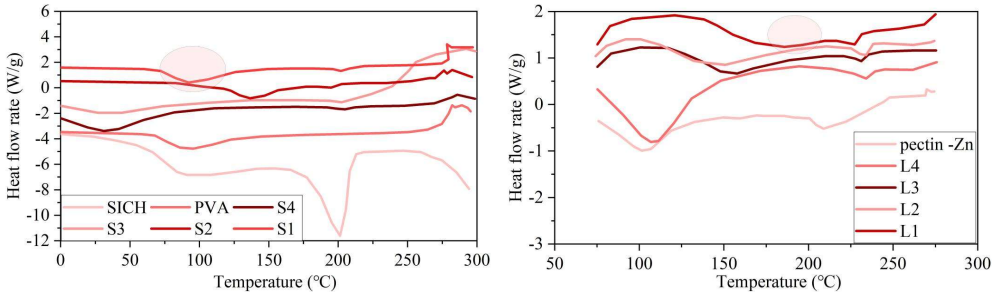


(a) DSC curves of SICH, PVA and cross-linked hydrogels

(b) DSC curves of pectin -Zn and cross-linked hydrogels

Figure 3: DSC curves of SICH, PVA, pectin -Zn and cross-linked hydrogel

## III. Drug delivery practices for cross-linked hydrogels

In this chapter, the cytotoxicity and biocompatibility of SICH hydrogels are determined. After that, the specific behavior of SICH hydrogel in drug delivery system for in vivo and in vitro drug release is investigated by rat experiments.

### *III. A. Cytotoxicity and biocompatibility of SICH hydrogels*

To investigate whether SICH hydrogel is cytotoxic, MTT cytotoxicity assay was performed on normal human skin fibroblasts (NHDF). The results of the MTT cytotoxicity assay of SICH hydrogel are shown in Figure 4.SICH hydrogel exhibited very low cytotoxicity against cultured NHDF cells, showing at least 70.49% cell viability at the highest

polymer concentration of 125 μg/mL.The SICH hydrogel (S3) showed 70.49% cell viability at 125 pg/mL, and cell viability gradually increased to 88.06% at 25 pg /mL, the cell viability gradually increased to 88.06%. SICH hydrogel (S2) showed lower cytotoxicity compared to SICH hydrogel (S3), with 88.06% cell viability at 125 pg/mL and 81.20% cell viability at 25 μg/mL.SICH hydrogel (S1) showed 86.68% and 91.35% cell viability at 125 pg/mL and 25 pg/mL, respectively , with a slight increase in cell viability compared to SICH hydrogel (S2). The present findings suggest that SICH hydrogels can be used as generally safe and non-toxic biomaterials for biomedical applications for drug delivery.

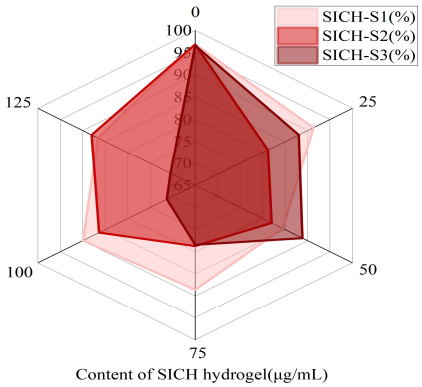


Figure 4: MTT-cellcytotoxicity assay of SICHs

### *III. B. Study of drug delivery behavior of cross-linked hydrogels*

#### III. B. 1) In vivo drug release behavior studies

Comparison of cross-linked (SICH) hydrogels and polyvinyl alcohol (PVA) hydrogels in drug delivery to validate the drug delivery advantages of SICH hydrogels. Figure 5 shows the in vivo drug release of the two hydrogel patches. Figure 5(a) shows the in vivo drug release assay to determine the amount of drug absorbed by rats by measuring the residual drug loading of SICH hydrogel or PVA hydrogel patches attached to the skin on the back of rats at different times. After insertion into the skin, the drug in the SICH hydrogel was rapidly released by about 12.5% in the first hour, followed by a slow release up to about 32.5% in the next 23 hours, which was nearly about three times higher than the release from the PVA hydrogel patch (10.55%) during the 24-hour treatment period. In addition by examining the cumulative amount of drug deposited in the skin in Figure 5(b) it can be seen that the amount of drug in the skin was above 175 μg/cm² most of the time with the SICH hydrogel, whereas in the PVA hydrogel patch group the amount was below 75 μg/cm² during the 24h period. Significantly higher amounts of drug were found to be retained in the SICH hydrogel skin compared to the PVA hydrogel patch (with an equivalent amount of drug) at all time points. These in vivo results confirm that a cross-linked SICH hydrogel-based drug delivery system can significantly improve drug delivery efficiency compared to PVA hydrogel patches.

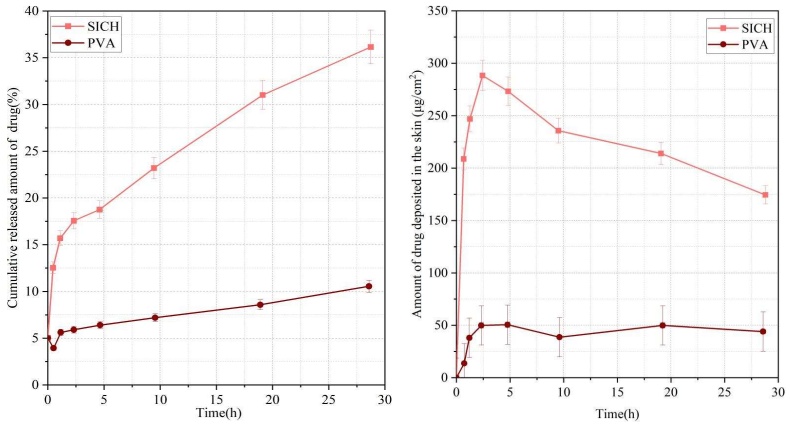


(a) Amount of drug released by the patch in the body of the skin

(b) Cumulative skin deposition amount of the drug released by the patch

Figure 5: Drug release in the body

### III. B. 2) Detachable SICH hydrogel microneedle drug load determination

In order to study the in vitro drug release behavior of SICH hydrogels, SICH hydrogels were fabricated into detachable SICH hydrogel microneedles and the drug loading in the microneedles was measured to ensure the validity of microneedle fabrication. Figure 6 shows the HPLC standard curve of drug content of SICH hydrogel microneedles. The standard curve about the drug was determined and y=35.60424x-62.21685 was obtained with $R^2$=0.06843, after determining that the drug loaded in a single needle was more than 60 μg. The reason for this may be attributed to the fact that the matrix material of the SICH hydrogel microneedle has a certain protective effect on the drug, which improves its storage stability.

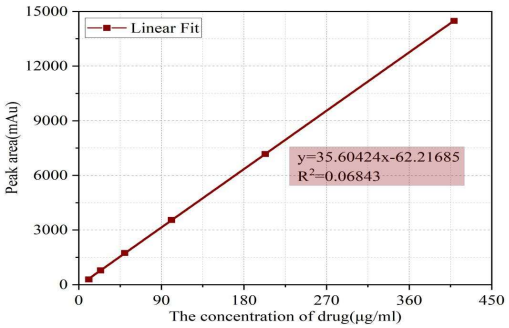


Figure 6: HPLC standard curve of drug content

### III. B. 3) In vitro drug release behavior study of detachable SICH hydrogel microneedles

Separable SICH hydrogel microneedles stabilized to contain drug were subjected to in vitro drug release behavior studies in rats. By partially embedding the drug-containing SICH hydrogel needle body in the rat subcutaneously, the SICH hydrogel absorbed water and dissolved to release the drug continuously using the concentration difference. Figure 7 shows the amount of drug released in vitro (37°C) measured using the Franz diffusion method test method. Analysis of Fig. 7 revealed that the drug was continuously released from the body of the needle for one day with rapid release up to 48.93% in the first 4 hours and continuous release up to 86.68% in the next 20 hours. In the in vitro release profile, the detachable SICH hydrogel microneedle did not show a burst release phenomenon, and the release profile was gentle, which realized the regulated release of the drug.

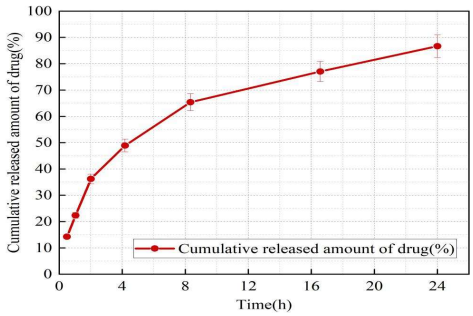


Figure 7: Drug release in vitro (37℃)

## IV. Conclusion

In this paper, we optimize the mechanical properties and biologically corresponding synergistic modulation effects of SICH hydrogels in drug delivery systems by introducing structure optimization algorithms such as GCNN into the design of cross-linked hydrogels. In the in vivo drug release behavior experiments, the drug in SICH hydrogel was slowly released to 32.5% in 24 hours, which is about three times higher than that of PVA hydrogel. And the drug content in the skin was above 175 μg/cm² most of the time, which was also higher than that of PVA hydrogel. When the drug was released in vitro, the drug in SICH hydrogel was released continuously for 24 hours, and the final release amount reached 86.68%, which had the release smoothness. Optimization of the molecular structure of cross-linked hydrogels using a structure optimization algorithm can improve their drug delivery effect. The cross-linking of different hydrogels can be further explored in the future to find more efficient and stable cross-linked hydrogels for accurate drug delivery.

## References


[1] Ghasemiyeh, P., & Mohammadi-Samani, S. (2019). Hydrogels as drug delivery systems; pros and cons. Trends in Pharmaceutical Sciences, 5(1), 7-24.

[2] Yu, Y., Xu, S., Li, S., & Pan, H. (2021). Genipin-cross-linked hydrogels based on biomaterials for drug delivery: A review. Biomaterials science, 9(5), 1583-1597.

[3] Kesharwani, P., Bisht, A., Alexander, A., Dave, V., & Sharma, S. (2021). Biomedical applications of hydrogels in drug delivery system: An update. Journal of Drug Delivery Science and Technology, 66, 102914.

[4] Ahmed, A. S., Mandal, U. K., Taher, M., Susanti, D., & Jaffri, J. M. (2018). PVA-PEG physically cross-linked hydrogel film as a wound dressing: experimental design and optimization. Pharmaceutical development and technology, 23(8), 751-760.

[5] Liu, X., He, X., Yang, B., Lai, L., Chen, N., Hu, J., & Lu, Q. (2021). Dual physically cross-linked hydrogels incorporating hydrophobic interactions with promising repairability and ultrahigh elongation. Advanced Functional Materials, 31(3), 2008187.

[6] Che, Y., Li, D., Liu, Y., Ma, Q., Tan, Y., Yue, Q., & Meng, F. (2016). Physically cross-linked pH-responsive chitosan-based hydrogels with enhanced mechanical performance for controlled drug delivery. RSC advances, 6(107), 106035-106045.

[7] Yang, J., Chen, Y., Zhao, L., Zhang, J., & Luo, H. (2023). Constructions and properties of physically cross-linked hydrogels based on natural polymers. Polymer Reviews, 63(3), 574-612.

[8] Iglesias, N., Galbis, E., Valencia, C., Díaz-Blanco, M. J., Lacroix, B., & de-Paz, M. V. (2020). Biodegradable double cross-linked chitosan hydrogels for drug delivery: Impact of chemistry on rheological and pharmacological performance. International Journal of Biological Macromolecules, 165, 2205-2218.

[9] Konieczynska, M. D., & Grinstaff, M. W. (2017). On-demand dissolution of chemically cross-linked hydrogels. Accounts of chemical research, 50(2), 151-160.

[10] Guaresti, O., García–Astrain, C., Palomares, T., Alonso–Varona, A., Eceiza, A., & Gabilondo, N. (2017). Synthesis and characterization of a biocompatible chitosan–based hydrogel cross–linked via 'click'chemistry for controlled drug release. International journal of biological macromolecules, 102, 1-9.

[11] Mali, K. K., Dhawale, S. C., Dias, R. J., Dhane, N. S., & Ghorpade, V. S. (2018). Citric Acid Crosslinked Carboxymethyl Cellulose-based Composite Hydrogel Films for Drug Delivery. Indian Journal of Pharmaceutical Sciences, 80(4).

[12] Wang, Y., Jiang, X., Li, X., Ding, K., Liu, X., Huang, B., ... & Xu, W. (2023). Bionic ordered structured hydrogels: structure types, design strategies, optimization mechanism of mechanical properties and applications. Materials Horizons, 10(10), 4033-4058.

[13] Li, Z., Song, P., Li, G., Han, Y., Ren, X., Bai, L., & Su, J. (2024). AI energized hydrogel design, optimization and application in biomedicine. Materials Today Bio, 101014.

[14] Zong, T., Liu, X., Zhang, X., & Yang, Q. (2024). Efficient characterization of double-cross-linked networks in hydrogels using data-inspired coarse-grained molecular dynamics model. The Journal of Chemical Physics, 160(2).

[15] Karaoglu, I. C., Kebabci, A. O., & Kizilel, S. (2023). Optimization of gelatin methacryloyl hydrogel properties through an artificial neural network model. ACS Applied Materials & Interfaces, 15(38), 44796-44808.

[16] Negut, I., & Bita, B. (2023). Exploring the potential of artificial intelligence for hydrogel development—a short review. Gels, 9(11), 845.